

THE INTERACTING EARLY-TYPE BINARY BD +40°4220 (V729 CYG): MODELING THE COLLIDING WINDS REGION¹

G. RAUW² AND J.-M. VREUX

Institut d’Astrophysique et de Géophysique, Université de Liège, 5, Avenue de Cointe, B-4000 Liège, Belgium

AND

B. BOHANNAN

Kitt Peak National Observatory, National Optical Astronomy Observatories,³ PO Box 26732, Tucson, AZ 85726-6732

Received 1998 September 2; accepted 1998 December 29

ABSTRACT

We present an analysis of an extensive set of spectroscopic observations of the mysterious early-type binary BD +40°4220. A new orbital solution is derived from the radial velocities of the absorption lines. We confirm that the secondary star is highly overluminous for its mass. The absorption lines of both components display phase-locked profile variations, with some of the secondary’s lines going into emission between $\phi = 0.20$ and $\phi = 0.55$. A detailed investigation of the profile variability of the He II $\lambda 4686$ emission line reveals that the pattern of variability of this line is very stable. We show that part of the He II $\lambda 4686$ emission is produced in the wind interaction region between the stars. Most of the emission lines in the visual spectrum of BD +40°4220 display variations that are reminiscent of those observed on the He II $\lambda 4686$ line, pointing toward a similar origin. We present numerical simulations of emission-line profiles in a colliding winds binary, showing that an important part of the variability observed in BD +40°4220 can be explained by a colliding winds phenomenon. The properties of the wind interaction region can be accounted for if we assume that the secondary star is an evolved object, most probably some kind of Ofpe/WN9 transition star, with a mass loss rate of $\sim 5.5 \times 10^{-6} M_{\odot} \text{ yr}^{-1}$. We finally discuss the fundamental parameters of the binary, concluding that mass transfer must have played a crucial role in the evolution of this system.

Subject headings: binaries: eclipsing — binaries: spectroscopic — stars: early-type — stars: individual (BD +40°4220) — stars: mass loss

1. INTRODUCTION

BD +40°4220 (V729 Cyg, Cyg OB 2 n°5) is an eclipsing binary with an orbital period of 6.6 days (Hall 1974). The system is a member of the heavily reddened association Cyg OB 2, which contains a wealth of massive and luminous stars (Massey & Thompson 1991). Walborn (1973) assigned a spectral type O7 Ia nfp to BD +40°4220. Based on the intensity ratio of the He I $\lambda 4471$ and He II $\lambda 4542$ absorption lines of each component, Bohannan & Conti (1976) derived spectral types O7 and O6 for the primary and secondary, respectively. These authors also classified both components as Of stars, since each of them seems to contribute to the He II $\lambda 4686$ emission. Moreover, since both components display absorption lines of similar strength, Bohannan & Conti (1976) concluded that the system is formed by two supergiants with nearly equal luminosities. On the other hand, their radial velocity curves led to a mass ratio of 4.3 ± 0.5 , suggesting that the secondary component must be highly overluminous for its mass. Bohannan & Conti (1976) therefore proposed that the secondary star in BD +40°4220 might be on its way to becoming a Wolf-Rayet star. Massey & Conti (1977) reinvestigated the orbital solution of BD +40°4220 and derived a somewhat lower mass ratio of 3.27. However, the discrepancy between the luminosity and the mass of the secondary star could not be solved.

¹ All the observations reported here were obtained at the Observatoire de Haute Provence and at the Kitt Peak National Observatory.

² Chargé de Recherches au Fonds National de la Recherche Scientifique (Belgium).

³ The National Optical Observatories are operated by the Association of Universities for Research in Astronomy, Inc. (AURA) under cooperative agreement with the National Science Foundation.

A completely different picture of BD +40°4220 arose from the analysis of its light curve by Leung & Schneider (1978). These authors suggested that BD +40°4220 might be an evolved contact system, with the primary about 2.1 mag brighter in the visual than the secondary. Such a luminosity ratio is in good agreement with the mass ratio, but is inconsistent with the observed strong spectral signature of the secondary. Leung & Schneider proposed that the primary might be the most evolved component of the system. They speculated that the strong spectral signature of the secondary reflects an unusual relationship between its luminosity and line strength, resulting from the presence of an extended envelope formed by material lost by the primary.

Vreux (1985) argued that the radial velocity variations of the strongest subpeak of the H α emission profile are indicative of material falling on a limited portion of the secondary’s surface. He suggested that either this material could be swept by the secondary during its motion across the primary’s wind, or it could come from a genuine mass transfer through “Roche lobe overflow” of the primary. The existence of such an interaction allows speculation on the possible effects of an additional “hydrogen cloaking” around the evolved secondary. Such a cloaking could play a key role in explaining the discrepancy between the spectral characteristics on one hand and the results of the radial velocity and photometric analyses on the other. Vreux (1985) suggested that the secondary could be a genuine Wolf-Rayet star, looking like an Of star because of the accretion of material from the primary.

Although the existence of profile variability of the He II $\lambda 4686$ emission line in the spectrum of BD +40°4220 was

TABLE 1
JOURNAL OF OBSERVATIONS AND RADIAL VELOCITY MEASUREMENTS OF BD +40°4220

DATE (JD 2440000.)	ϕ^a	INSTRUMENT ^b	SPECTRAL RANGES ^c	N ^d	RADIAL VELOCITY ^e	
					Primary (km s ⁻¹)	Secondary (km s ⁻¹)
9551.526	0.968	E	3850–6800	1	...	-88.4
9552.528	0.120	E	3850–6800	1	-54.9	89.5
9553.528	0.272	E	3850–6800	1	-107.7	...
9559.477	0.173	C	H α	1	-134.1	193.9
9560.526	0.332	C	H α	1	-97.0	221.7
9576.436	0.743	C	3920–4380	2	48.6	-318.6
9577.456	0.898	C	3920–4380	1	19.8	-313.1
9578.480	0.053	C	3920–4380	1	-110.2	-28.5
9579.469	0.203	C	3920–4380	1	-102.9	202.3
9580.545	0.366	C	3920–4380	1	-110.7	136.4
9581.459	0.505	C	3920–4380	2	...	-69.5
9582.446	0.654	C	3920–4380	2	31.8	-207.3
9583.445	0.806	C	3920–4380	2	25.7	-357.2
9911.501	0.528	C	He II, H β , He I	8	-0.7	-105.9
9912.435	0.669	C	He II, H β , He I	8	23.2	-273.3
9913.503	0.831	C	He II, H β , He I	8	35.6	-310.2
9914.397	0.967	C	He II, H β , He I	6	-48.9	-213.9
9915.435	0.124	C	He II, H β , He I	7	-90.0	71.3
9915.791	0.178	K	4320–4920	2
9916.545	0.292	C	He II, H β , He I	8	-98.8	...
9917.461	0.431	C	He II, H β , He I	9	-47.2	...
9917.837	0.488	K	4320–4920, 5570–6170	5
9918.810	0.635	K	4320–4920	2
10298.470	0.331	A	4670–4870	1
10299.466	0.482	A	4560–4970	1
10315.476	0.765	A	4110–4950	2	38.4	-384.8
10316.342	0.888	A	4110–4950	1	30.1	-289.1
10318.390	0.198	A	4110–4950	2	-118.3	...
10638.377	0.697	A	4110–4950	1	59.4	-303.2
10639.409	0.854	A	4110–4950	1	60.1	-332.4
10640.437	0.010	A	4110–4950	1	-34.6	-34.6
10641.446	0.163	A	4110–4950	1
10642.425	0.311	A	4110–4950	1	...	170.6
10643.443	0.465	A	4110–4950	1	-58.3	34.1

^a Orbital phases are computed using Hall's (1974) photometric ephemeris: 2440413.796 + 6 d 5977915E.

^b Different letters indicate different spectrographs: E = Elodie (OHP), C = Carelec (OHP), K = Coudé CCD Spectrograph (KPNO), A = Aurélie (OHP). See text for a detailed description of the instrumental configuration.

^c The different wavelength ranges are H α , 6350–6800 Å; He II, 4530–4720 Å; H β , 4750–4950 Å; and He I, 5650–6100 Å.

^d Number of spectra obtained during a night.

^e Last two columns list the mean heliocentric radial velocities determined from the absorption lines of each component.

already suspected by Bohannan & Conti (1976), there has been no dedicated phase-resolved analysis of the phenomenon until the work of Vreux et al. (1996) and Rauw (1997). Vreux et al. (1996) showed that the He II λ 4686 emission peak displays a behavior reminiscent of the H α subpeak studied by Vreux (1985). They therefore concluded that both lines are at least partially formed in the same physical region, i.e., between the two stars, possibly near the equilibrium surface of the colliding winds of both components.

Radio observations of BD +40°4220 over the last 20 yr revealed many interesting properties of this system. Abbott, Bieging, & Churchwell (1981) observed BD +40°4220 with the VLA in the highest resolution mode and detected two radio sources: the main component lying at the position of BD +40°4220 and a fainter source located at 0.9 from the binary system. Subsequent observations indicated that the

radio emission of the main source is variable on a timescale of about 7 yr between a low state and a high state (Miralles et al. 1994). During the high state, the radio emission is nonthermal, while it becomes essentially thermal during the low state. Recent high-resolution VLA and *Hipparcos* observations of BD +40°4220 by Contreras et al. (1997) indicate that the second radio source near BD +40°4220 is not associated with the faint optical companion ($m_V \sim 13$) discovered by Herbig (1967); rather, it lies between BD +40°4220 and the visual companion. Contreras et al. (1997) interpret the second radio source as having been formed in the shock-interaction zone between the winds of BD +40°4220 and the faint companion.

In the present paper we discuss an extensive set of spectroscopic observations of BD +40°4220 and extend the preliminary analysis presented by Vreux et al. (1996). We

focus on the phase-locked line profile variability that arises in the close binary system as a consequence of the strong interaction between the two components. Starting with the absorption lines, we first derive an improved orbital solution and discuss the orbital variability of these lines in § 3. As a next step, in §§ 4 and 5 we examine the variations of the emission lines, and in § 6 we make use of a dedicated numerical code to simulate the variability of the He II $\lambda 4686$ line resulting from the wind interaction. Finally, in § 7 we discuss the evolutionary status of the two components of the close binary.

2. OBSERVATIONS AND DATA REDUCTION

Spectroscopic observations of BD +40°4220 were collected during several observing campaigns between 1994 and 1997 with various instruments at the Observatoire de Haute-Provence (OHP) and the Kitt Peak National Observatory (KPNO). The journal of observations is given in Table 1.

A few spectra were taken in 1994 July with the fiber-fed échelle spectrograph Elodie (Baranne et al. 1996), mounted on the 1.93 m telescope at OHP. The detector was a back-side-illuminated TK1024 CCD, with a pixel size of 24 μm , providing a resolving power of 45,000. The typical exposure time was 30 minutes, leading to a S/N ratio of ~ 50 per pixel at 6000 Å. Because of the strong reddening of BD +40°4220, the S/N ratio below ~ 5500 Å is not sufficient to study line variability. A more extensive set of observations was secured with the Carelec spectrograph attached to the same telescope in 1994 and 1995. The detector was a Tektronix TK512 CCD, with a pixel size of 27 μm . The violet (3920–4380 Å) spectra were obtained with a 1200 lines mm^{-1} grating blazed at 4000 Å, providing a reciprocal dispersion of 33 Å mm^{-1} . The spectral resolution as derived from the FWHM of the lines in the calibration exposures is 1.63 Å. Additional spectra were obtained with a 1200 lines mm^{-1} grating blazed at 7500 Å. Four different wavelength domains, centered on $\lambda 4600$, H β , He I $\lambda 5876$, and H α , were investigated. The blue settings were observed in the second order with a reciprocal dispersion of 17 Å mm^{-1} , while the yellow and red settings were observed in the first order with a reciprocal dispersion of 33 Å mm^{-1} . The spectral resolutions measured on the calibration exposures are 0.68, 1.64, and 1.30 Å, respectively, for the blue domains, the He I $\lambda 5876$ and H α settings. In 1995 July, several spectra were taken simultaneously with the OHP campaign at the Coudé Feed telescope of the Kitt Peak National Observatory. The detector was a Ford 3K \times 1K thinned CCD, with a pixel size of 15 μm . The spectra were taken with a 316 lines mm^{-1} grating blazed at 12,000 Å (grating B) in the second order, providing a reciprocal dispersion of 14.8 Å mm^{-1} . The instrumental configuration led to a resolving power of ~ 7500 in the blue (4320–4920 Å) and $\sim 10,000$ in the yellow (5570–6170 Å). Finally, additional observations were gathered in 1996 and 1997 with the Aurélie spectrograph (Gillet et al. 1994), fed by the 1.52 m telescope at OHP. The detector was a Thomson TH7832 linear array with a pixel size of 13 μm . Two snapshot spectra were taken with a 1200 lines mm^{-1} and a 600 lines mm^{-1} grating, both blazed at 5000 Å and providing resolutions of 0.31 and 0.61 Å, respectively, over the wavelength ranges 4670–4870 Å and 4560–4970 Å. Eleven more spectra were obtained with a 300 lines mm^{-1} grating blazed at 6000 Å, providing a reciprocal dispersion of 33 Å mm^{-1} over a wavelength

range from 4110 to 4950 Å. The spectral resolution as derived from the FWHM of the calibration lines is 1.20 Å. Given the severe reddening toward BD +40°4220, the mean exposure times strongly depend on the observed spectral range. Typically, a S/N ~ 100 was achieved within 1 hr in the blue-violet domains, while the same result was obtained within 5 minutes in the H α setting.

All the data were reduced in the standard way using the MIDAS package developed at ESO. The spectral band between 5860 and 5980 Å is affected by absorption bands of telluric water vapor. A template of the telluric spectrum was constructed by observing the star HD 200340 (B6 V, $m_V = 6.5$) at very different air masses. This template was then used for a first-order correction of the telluric features.

3. ANALYSIS OF THE ABSORPTION LINES

3.1. Radial Velocities

As a first step, we have determined a new orbital solution for BD +40°4220. The radial velocities of the absorption lines of both components were determined by fitting Gaussians whenever the separation between the two components was sufficient to do so. The mean radial velocities (RVs) are listed in Table 1. The orbital phases were computed using the photometric ephemeris of Hall (1974). The present data set provides a much denser phase coverage of the orbital cycle than any previous investigation. Some of our data have already been used by Vreux et al. (1996) to derive a preliminary orbital solution.

The determination of the orbital elements of this system is complicated by the fact that the absorption lines of the two components appear to be sometimes heavily blended, even at orbital phases when this situation is not expected (i.e., in the phase interval [0.2, 0.4]; see Rauw 1997 and § 3.3 below).

Since the orbital period of BD +40°4220 is rather short and since there is no indication of a nonzero eccentricity in the light curve, we have assumed a circular orbit. We have computed two different least-squares orbital solutions using either our new RVs alone or our RVs together with the data of Bohannan & Conti (1976). The results are described in Table 2, and the latter solution is shown in Figure 1. Using the entire data set, we can check that there is no systematic difference (e.g., in orbital phase) between the two epochs. The two solutions shown in Table 2 agree within their errors, and in the following discussion we will consider the solution derived from the whole data set. In Table 2 we provide an estimate of the radii of the Roche lobes corresponding to the mass ratio q determined from the orbital solutions. However, one has to bear in mind that the “classical” Roche lobe is not necessarily appropriate to describe the equipotentials in an early-type binary such as BD +40°4220, where radiation pressure is likely to play a crucial role (Drechsel et al. 1995; Kondo 1996).

In the present analysis, we consider the apparent systemic velocity of each component as a free parameter of the orbital solution. In their study of BD +40°4220, Bohannan & Conti (1976) assumed both stars to have identical systemic velocities. However, dropping this assumption, Massey & Conti (1977) achieved an orbital solution with quite different apparent systemic velocities for the two stars and derived a different mass ratio. We find that the secondary’s absorption lines yield a considerably more negative apparent systemic velocity than those of the primary, indi-

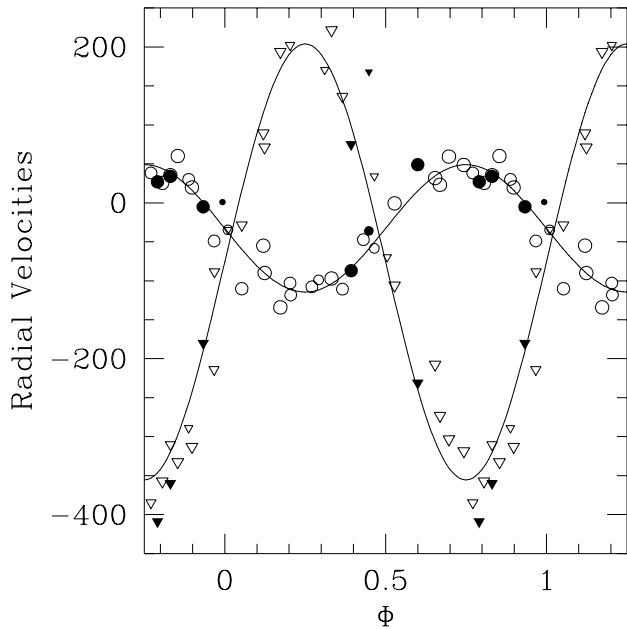


FIG. 1.—Radial velocity curves of BD +40°4220. Circles and triangles stand for the RV's of the absorption lines of the primary and the secondary, respectively. Open symbols indicate our new data; filled symbols stand for the data of Bohannan & Conti (1976). The size of the symbols yields the weighting of the data in the least-squares solution, larger symbols indicating higher weights.

cating that the former lines are probably (at least partially) formed in the secondary's wind. We further notice a group of points in the phase interval $\sim[0.60, 0.75]$ that yield observed RVs of the secondary star that are systematically less negative than expected from the least-squares solution. As we will see in § 5, it is during these orbital phases that we observe the hemisphere of the secondary star where the velocity law of the wind is the most affected by the proximity of the wind interaction (see Fig. 11). It is therefore very likely that the less negative RVs of the secondary indicate a slower wind from that part of the surface, a situation that is also expected from theoretical considerations (Stevens & Pollock 1994).

The minimum masses of the two stars as derived here are about a factor of 1.3 lower than the values previously found by Massey & Conti (1977).

3.2. Spectral Types and Luminosity Ratio

We have measured the equivalent widths of several absorption lines of both components whenever they were clearly separated (Table 3 and Rauw 1997). When considering these values, one has to be aware that at least some of the absorption lines, especially those of the secondary star, are partially filled in by circumstellar emission (see § 3.3).

Following Conti (1973), we use the ratio W of the equivalent widths of the He I $\lambda 4471$ and He II $\lambda 4542$ absorption

TABLE 2
ORBITAL ELEMENTS OF BD +40°4220

PARAMETER	NEW RVs ONLY		ALL RV DATA	
	Primary	Secondary	Primary	Secondary
K (km s $^{-1}$)	82.2 ± 3.5	272.3 ± 8.7	79.1 ± 3.2	279.7 ± 8.3
γ (km s $^{-1}$)	-33.2 ± 2.9	-72.7 ± 7.0	-30.8 ± 2.6	-75.8 ± 6.4
$m \sin^3 i$ (M_\odot)	23.3 ± 2.3	7.0 ± 0.8	24.6 ± 2.5	6.9 ± 0.6
$q = m_{\text{Prim}}/m_{\text{Sec}}$	3.31 ± 0.25	3.31 ± 0.25	3.54 ± 0.18	3.54 ± 0.18
$a \sin i$ (R_\odot)	10.7 ± 0.5	35.4 ± 1.1	10.3 ± 0.4	36.4 ± 1.1
$R_{\text{RL}} \sin i$ (R_\odot) ^a	22.3	12.9	22.9	12.9

NOTE.—Orbital solution computed from the mean RVs of the absorption lines assuming a circular orbit. The quoted errors are 1σ uncertainties.

^a The radii of the classical Roche lobes are computed using the formula given by Eggleton (1983).

TABLE 3
EQUIVALENT WIDTHS OF PROMINENT ABSORPTION LINES IN THE SPECTRUM OF BD +40°4220.

LINE	MEAN EW		MEAN INTENSITY RATIO ^a	PHASE INTERVAL ^b
	Primary (Å)	Secondary (Å)		
He I $\lambda 4026$	0.11	0.19	0.6 ± 0.2	0.65–0.81
He II $\lambda 4200$	0.14	0.06	2.3 ± 0.2	0.65–0.74
H γ	0.29	0.18	1.5 ± 0.8	0.74–0.90
He I $\lambda 4471$	0.22	0.16	1.5 ± 0.4	0.63–0.86
He II $\lambda 4542$	0.28	0.29	1.0 ± 0.2	0.67–0.83

^a Mean intensity ratio: primary/secondary.

^b Phase interval over which the line intensities of both components could be measured.

lines as the primary classification criterion among O stars. From our data, we derive spectral types of O6.5–7 for the primary ($W = 0.75 \pm 0.06$) and O5.5–6.5 for the secondary ($W = 0.56 \pm 0.12$). These estimates are in fair agreement with the spectral types provided by Bohannan & Conti (1976).

Table 3 summarizes the measured equivalent width ratios of absorption lines from the two components. The He I and He II absorption-line ratios indicate somewhat different luminosity ratios, a not unexpected result given the various degrees of wind contamination and the slightly different spectral types of the two components. On average, we derive a spectroscopic luminosity ratio of the two components of 1.4 ± 0.6 . The latter value is obviously at odds with the orbital solution, a result consistent with the same luminosity problem found by Bohannan & Conti (1976). Indeed, for such early-type stars, a mass ratio of 3.5 is expected to correspond to a bolometric luminosity ratio of about 50, and hence a luminosity ratio of 6–8 in the visual.

3.3. Variability

Bohannan & Conti (1976) noticed that some of the secondary's absorption lines appear weaker when the secondary is moving away from the observer. A similar phenomenon, called the *Struve-Sahade effect*, was found in several other early-type binaries containing at least one evolved component that undergoes mass loss or mass exchange (Stickland 1997; Gies, Bagnuolo, & Penny 1997). In the case of AO Cas (O9.5 III + O8 V), Gies et al. (1997) suggest that the Struve-Sahade effect results from preferential photospheric heating of the secondary's hemisphere facing the bow shock, produced by the stellar winds' collision. Our observations confirm that the properties of the absorption lines in the spectrum of BD +40°4220 suffer phase-locked variability. For instance, during the phase interval $\sim [0.2, 0.3]$, the lines of *both* stars appear systematically broader, and although their RV separation should be sufficient to resolve the lines, they are heavily blended.

Whereas the He II $\lambda 4542$ lines of both components remain in absorption over the whole orbital cycle, several lines of the secondary (H γ , He I $\lambda\lambda 4026, 4471, 4713$, and He II $\lambda 4200$) that appear most of the time in absorption go into emission between $\phi \simeq 0.05$ and $\phi \simeq 0.55$ (see Rauw 1997). These emission components are shifted toward the red with respect to the secondary's RV curve as derived from the absorption lines. As an illustration, the variability of the H γ line is displayed in Figure 2. The primary's line remains always in absorption. In the phase interval $[0.65, 0.90]$, a second, strongly variable, blueshifted absorption line is seen, a feature that can be associated with the secondary star. Between $\phi \simeq 0.054$ and $\phi \simeq 0.505$, the secondary's absorption disappears, and we observe a redshifted emission line instead.

At first sight, a situation like this could be expected if the intrinsic profiles of the secondary's lines were of P Cygni type. In this case, the primary's absorption line and the secondary's emission would be blended between phases $\phi \simeq 0.60$ and $\phi \simeq 0.90$, i.e., when the secondary is approaching and, as a net result, the secondary's emission component would therefore be attenuated. However, a quantitative correction of the contribution of the primary's absorption to the observed blend (see § 4.2 and Rauw 1997) indicates that the profile of the restored line of the secondary is not of P Cygni type, at least not over the entire orbital

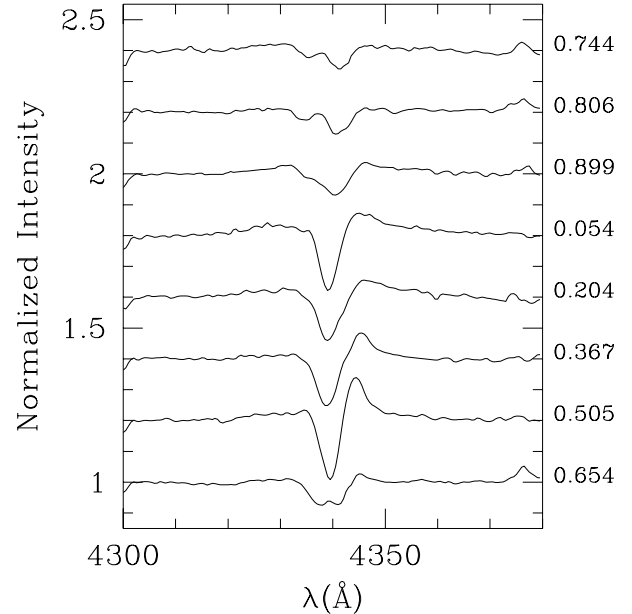


FIG. 2.—Variations of the H γ line in the spectrum of BD +40°4220 as observed in 1994 August. Orbital phases are indicated on the right. The faint emission that appears at certain points (0.744, 0.806, 0.899, and 0.654) near the red edge of the spectral domain is due to N III $\lambda 4379$. Note also the broad emission underlying the H γ profile.

cycle. The explanation could be that the secondary's wind, where the emission component arises, is compressed by the bow shock resulting from the wind interaction (see § 5).

4. THE EMISSION LINES

All the emission lines in the visible spectrum of BD +40°4220 exhibit phase-locked profile variations. Vreux (1985) studied the variability of the H α line, and Vreux et al. (1996) presented a preliminary analysis of the He II $\lambda 4686$ line. Among the emission lines we have observed, He II $\lambda 4686$ displays the simplest behavior and is thus the best suited for a tailored modeling of the phenomenon. In this section, we therefore present a more detailed discussion of this line and extend our analysis to several other lines showing more complicated deformations.

4.1. He II $\lambda 4686$

The most prominent intensity variations and profile deformations arise in the central part of the line (Fig. 3). The emission peak displays radial velocity variations that are shifted in phase between the orbital solutions of the primary and the secondary (Fig. 4).

To study these RV variations, we have used a technique based on the so-called "S-wave analysis" (e.g., Richards, Jones, & Swain 1996 and references therein). We adopt a reference frame attached to the center of mass of the binary. The x-axis points toward the secondary, and the y-axis points in the direction of the secondary's orbital motion. The spectral signature of an emitting volume characterized by a stationary velocity vector in this coordinate system describes a sinusoidal RV curve as a function of orbital phase:

$$v(\phi) = -v_x \cos(2\pi\phi) + v_y \sin(2\pi\phi) + v_z. \quad (1)$$

In the case of cataclysmic variables and Algol binaries, a least-squares determination of the (v_x, v_y) velocities of a dis-

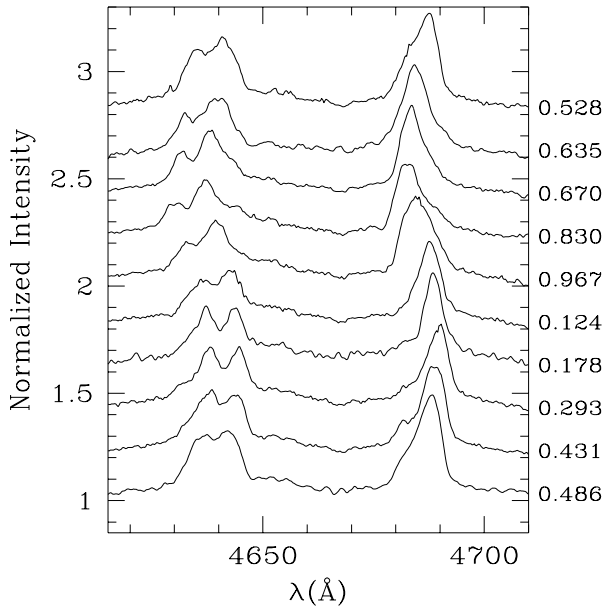


FIG. 3.—Variability of the He II $\lambda 4686$ and N III $\lambda\lambda 4634, 4640-41$ emission lines in the spectrum of BD +40°4220 as observed in 1995 July.

crete emission component yields important information on the properties of the emitting region and the mass exchange processes. In the case of early-type binaries, the situation is more complex because of the presence of the stellar winds, and we have therefore included a third component, v_z , in the S-wave analysis, mainly to take into account the differences in systemic velocity for various lines.

For the emission peak of the He II $\lambda 4686$ line, the best fit is achieved for $v_x = 74 \pm 7$, $v_y = 218 \pm 7$, and $v_z = 28 \pm 5$ km s^{-1} . This result is illustrated in Figure 4, along with the

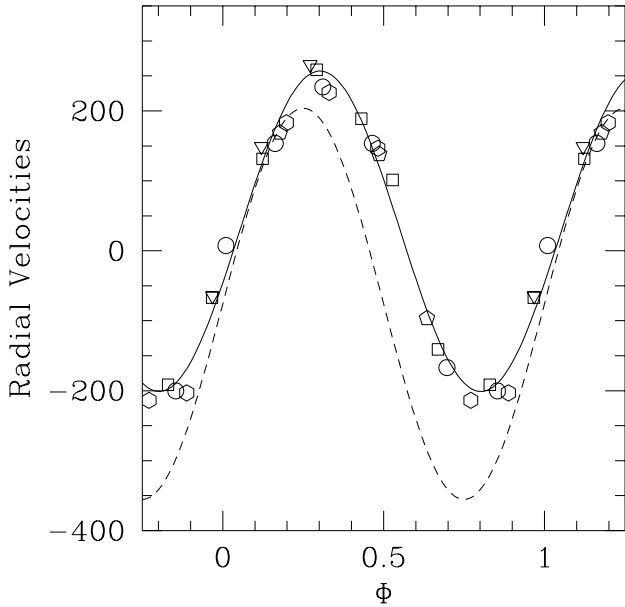


FIG. 4.—Radial velocity variations of the He II $\lambda 4686$ emission peak in the spectrum of BD +40°4220. The different symbols indicate data collected with different instruments and/or at different epochs: triangles, Elodie 1994; squares, Carelec 1995; pentagons, KPNO 1995; hexagons, Aurélie 1996; circles, Aurélie 1997. The solid line indicates the best fit to the data using equation (1). For comparison, the dashed line illustrates the least-squares RV curve of the secondary's absorption lines.

orbital solution of the secondary as derived from the RVs of its absorption lines (§ 3.1). Comparing the RV curve of the He II $\lambda 4686$ emission to the secondary's least-squares orbital solution, we notice that the former has a lower amplitude (230 versus 280 km s^{-1}) and lags behind the latter by some +0.05 in phase.

In the winds of early-type stars, the He II $\lambda 4686$ emission line is formed through recombination in regions with a relatively high density. In the case of an Of binary system, there can be up to three such zones: two in the inner parts of the individual winds and a third one in the wind-interaction region. The most likely interpretation of the RV curve of the He II $\lambda 4686$ peak is that the emission peak arises in the interaction region, i.e., in a volume of matter moving from the primary toward the secondary ($v_x > 0$). The large positive v_y value further implies that this volume is probably located close to the secondary star.

In order to derive additional constraints on the location of the line-emitting region, we have normalized the spectra in the wavelength range 4600–4720 Å in a uniform way and have measured the “equivalent widths” of the He II $\lambda 4686$ line integrated between $\lambda 4670$ and $\lambda 4705$. The resulting “light curve” is illustrated by the filled symbols in Figure 5. The estimated errors of these measurements are 0.10–0.15 Å. However, since BD +40°4220 is an eclipsing binary, the EWs measured in this way refer to a variable continuum level and thus do not reflect the apparent variations of the line-emitting volume. Therefore, we have used the light curve in the Johnson *B* filter provided by Leung & Schneider (1978) to correct the EWs for this effect. The resulting data points are shown by the open symbols in Figure 5. If the line-emitting volume is not affected by the occultations, the result of this operation should be a nearly constant EW. Outside the phase intervals [0.80, 0.20] and [0.40, 0.50], we indeed find a corrected EW that is roughly constant, with a mean value of 4.44 ± 0.10 Å. However, Figure 5 shows that during the phase interval [0.80, 0.20] the emitting volume undergoes a broad occultation that is slightly displaced (by $\sim +0.05$ in phase) with respect to the minimum of the *B* light curve and has a depth of about 0.8 Å (i.e., some 20% of

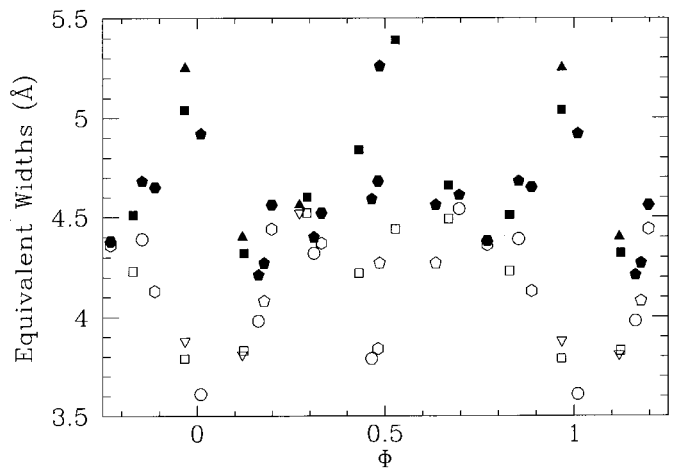


FIG. 5.—Equivalent width of the He II $\lambda 4686$ emission line, integrated on the normalized spectra between $\lambda 4670$ and $\lambda 4705$. The different symbols refer to various observing runs and have the same meanings as in Fig. 4. Filled symbols indicate the raw measurements, while open symbols indicate the EWs “corrected” for the varying continuum level using the *B* light curve of Leung & Schneider (1978).

the total corrected EW). Moreover, two data points from two different observing runs indicate that there is most probably another very narrow occultation around $\phi \simeq 0.47$. The light curve of the corrected EWs provides important constraints on the location of the line-emitting region. In fact, the broad minimum around $\phi = 0.05$ indicates that the line emission arises close to the secondary's surface, while the narrow occultation near $\phi = 0.47$ tells us that the emitting volume must be rather thin. Moreover, the slight phase shifts between the minima of the corrected EWs and those of the *B* light curve indicate that the emitting volume is not aligned with the axis of the binary system. These results are in fair agreement with the properties of the H α emission as derived by Vreux (1985). Although a complete quantitative analysis of the phenomenon must await the results of dedicated photometric observations, Rauw (1997) uses a simplified model of the emitting volume to simulate the light curve of the He II $\lambda 4686$ line. These simulations indicate that the emitting region has a thickness of about $0.1\text{--}0.2 R_\odot$ and that its center is located at a position angle of $\psi \sim 20^\circ$ with respect to the binary axis. The narrowness of the secondary occultation further indicates that the orbital inclination must be rather low, i.e., of the order of $50^\circ\text{--}60^\circ$ (Rauw 1997).

From these results, we conclude that a significant fraction of the line emission is produced in the interaction region between the two stars. We emphasize our finding that this interaction region precedes the secondary star on its orbit. In fact, in the case of a classical Roche lobe overflow of the primary, the impact of the mass flow is expected on the back side of the secondary star (Lubow & Shu 1975). The location of the interaction region in BD +40°4220 is therefore more consistent with either a focused wind (Stevens 1988) or a colliding winds phenomenon (e.g., Stevens, Blondin, & Pollock 1992).

Finally, Figure 6 shows the first-order moment,

$$W_1 = \left(\frac{c}{\lambda_0 v_\infty} \right)^2 \int_{\text{line}} (F_\lambda - 1)(\lambda - \lambda_t) d\lambda, \quad (2)$$

of the He II $\lambda 4686$ emission with respect to the wavelength of the emission peak λ_t and integrated between $\lambda 4670$ and $\lambda 4705$. F_λ is the normalized flux of the line, and λ_0 stands for the rest wavelength of the transition. The first-order moment provides a quantitative measure of the skewness of the line profile with respect to λ_t (Hutsemékers 1988). Figures 4, 5, and 6 demonstrate the amazing stability of the

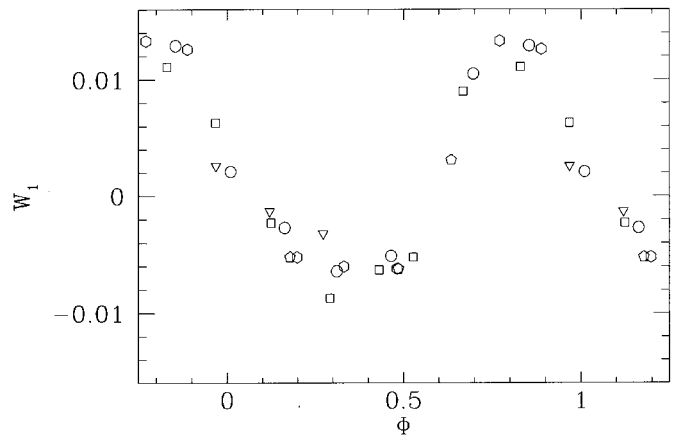


FIG. 6.—First-order moment of the He II $\lambda 4686$ emission line integrated on the normalized spectra between $\lambda 4670$ and $\lambda 4705$. Symbols have the same meaning as in Fig. 4. In these calculations we have adopted a terminal velocity of $v_\infty = 2000 \text{ km s}^{-1}$.

profile variability of the He II $\lambda 4686$ line over a timescale of at least 4 yr.

4.2. Other Emission Lines

In a comprehensive analysis of the phase-locked variability of the H α line, Vreux (1985) noticed that the strongest subpeak of the profile describes an RV curve indicating a formation on a limited part ($\sim 20\%$) of the secondary's surface facing the primary star. We have applied an S-wave analysis to the RVs measured by Vreux (1985) and our new data from the 1994 observing campaigns. The best-fit parameters, given in Table 4, are in qualitative agreement with the results of the He II $\lambda 4686$ line.

The variability of the H β line is illustrated in Figure 7. The profile is usually composed of at least two emission peaks and an absorption line with zero radial velocity in the frame of the primary star. On a few spectra taken when the secondary star approaches the observer (e.g., $\phi = 0.684$), we notice a very weak absorption with a velocity consistent with the orbital motion of the secondary star.

The He I $\lambda 5876$ line also displays rather complex variations. Nevertheless, if we consider the spectra in the reference frame of the primary star, we again notice an absorption component with zero velocity superimposed on a broad, complex, variable emission component. The He I $\lambda 5876$ line is therefore most likely in absorption in the spec-

TABLE 4
S-WAVE ANALYSIS OF VARIOUS EMISSION LINES IN THE SPECTRUM OF BD
+40°4220

Line	v_x (km s $^{-1}$)	v_y (km s $^{-1}$)	v_z (km s $^{-1}$)	$ O - C $ (km s $^{-1}$)
H α	100 ± 6	186 ± 4	61 ± 6	79
H β ^{a,b}	52 ± 8	110 ± 8	139 ± 6	30
He I $\lambda 5876$ ^a	12 ± 8	112 ± 9	175 ± 6	25
He II $\lambda 4686$	74 ± 7	218 ± 7	28 ± 5	21
N III $\lambda 4634$	90 ± 8	260 ± 8	38 ± 6	35
N III $\lambda 4640$	71 ± 8	226 ± 8	13 ± 6	19
Si IV.....	87 ± 9	223 ± 7	37 ± 6	42
C III $\lambda 5696$	4 ± 8	-45 ± 9	-67 ± 6	17

^a The RVs are measured on restored emission lines.

^b Only the 1995 observations were taken into account in the S-wave analysis.

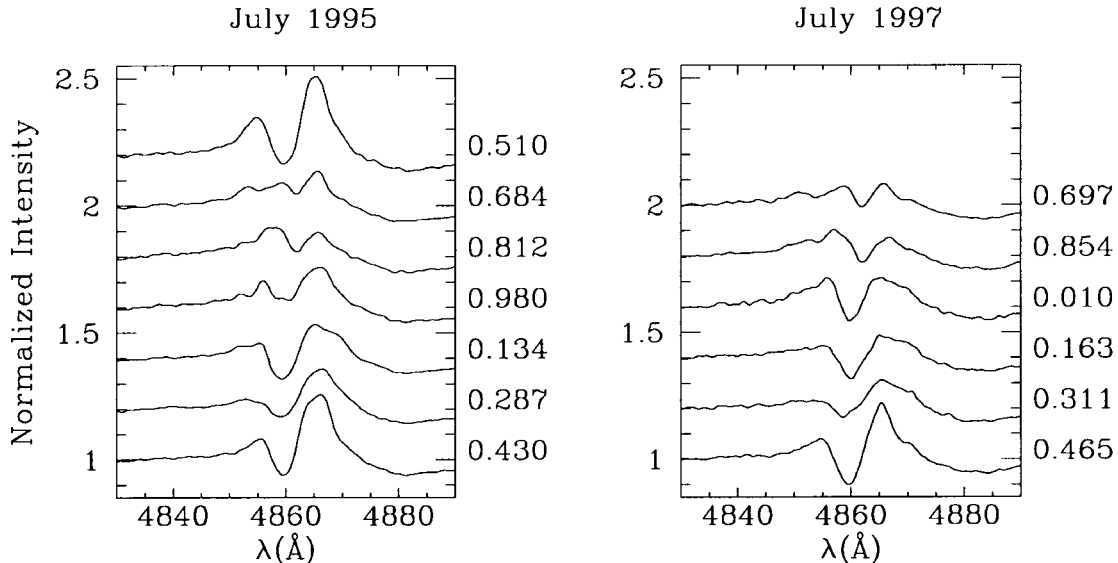


FIG. 7.—Variability of the H β line observed at different epochs. The orbital phases are indicated on the right.

trum of the primary star. Following a method outlined by Blake et al. (1995), we have attempted a first-order “restoration” of the H β and He I $\lambda 5876$ emission lines. To this end, we use the observed spectrum of the O8 If star HD 188001 (9 Sge) to build templates of the photospheric absorption lines. These reference profiles are broadened from the rotational velocity of HD 188001 ($v \sin i = 88-112$ km s $^{-1}$; Conti & Ebbets 1977; Penny 1996) to match the rotational velocity appropriate for the absorption lines of the primary star in BD +40°4220 (see Rauw 1997). The resulting absorption profiles are finally subtracted from the observed profiles of BD +40°4220. The best results are achieved for a rotational velocity of the primary component of 150 km s $^{-1}$, in reasonable agreement with the value of $v \sin i = 130$ km s $^{-1}$ suggested by Bohannan & Conti (1976). However, we noticed that the spectra taken between $\phi = 0.2$ and $\phi = 0.3$ display a broader absorption line, with $v \sin i$ of at least 200 km s $^{-1}$. This episodic broadening is also seen on other absorption lines of the primary (§ 3.3). Since the absorption lines of Of stars are at least partially formed in the wind, this broadening could reflect a major perturbation of the velocity law in the deeper layers of the primary’s wind, due to the proximity of the wind collision zone (Fig. 11).

For each line, we have measured the radial velocities of the strongest peak on the reconstructed emission profile and applied an S-wave analysis. The results derived from the 1994–1995 observations are listed in Table 4. Unlike the behavior of the He II $\lambda 4686$ line, the deformations of the H β line change between our first observations in 1995 and the subsequent (1996, 1997) runs. A detailed look at Figure 7 indeed reveals important quantitative differences. Attempts to restore the emission profile on spectra taken in 1996 and 1997 usually produce a multipeaked structure, rendering any RV measurement ambiguous. The reason for this failure is that while the emission component is generally weaker in the 1996 and 1997 data, the shape of the primary’s absorption line is no longer matched by our template, whatever value of the rotational velocity we adopt. Hydrodynamical instabilities in the colliding winds region between the two stars could be a possible explanation of the

changing amount of emission. Such instabilities are indeed predicted by hydrodynamic simulations (Stevens et al. 1992), but in such a case, the stability of the deformations of the He II $\lambda 4686$ line would be rather unexpected. Obviously, long-term monitoring of BD +40°4220 is needed to clarify the origin of the H β long-term variations and to search for a possible connection with other long-term changes, such as the 7 yr cycle in the radio emission (Miralles et al. 1994).

The blend of the N III $\lambda\lambda 4634, 4640-41$ lines displays a double-peaked emission structure. The separation and the intensities of both peaks change during the orbital cycle (Fig. 3). The results of the radial velocity analysis are provided in Table 4. Both components of the blend have RV curves with positive v_x and v_y , but we notice the slightly different locations of the line-emitting regions in the velocity space. We have measured the normalized intensities of the two peaks and corrected these measurements for the variations of the underlying continuum. The results are displayed in Figure 8. This figure clearly illustrates the different behavior of the two peaks. The intensity of the N III $\lambda\lambda 4640-41$ emission, i.e., the strongest component of the whole blend, shows variations that are a bit reminiscent of the light curve of the He II $\lambda 4686$ line. On the other hand, the N III $\lambda 4634$ line displays more ample and more regular variations, with a broad minimum at phase $\phi = 0.0$ and a maximum at $\phi = 0.3$. The mechanism of formation of the N III $\lambda\lambda 4634, 4640-41$ ($3p^2P^0-3d^2D$) lines in the spectra of O stars has been discussed by Mihalas & Hummer (1973). These authors have shown that in the photospheres of O((f)), O(f), and Of stars, the $3d$ level gets overpopulated by means of dielectronic recombination, leading to photospheric emission of the $\lambda\lambda 4634, 4640-41$ multiplet, whereas the $3s^2S-3p^2P^0$ ($\lambda\lambda 4097, 4103$) transition remains in absorption. In the case of Of stars, the emission at $\lambda 4634, 4640-41$ can be further enhanced by a “fluorescence” mechanism in the extended atmosphere of the star (Swings 1948). Our analysis of the RVs of the $\lambda\lambda 4634, 4640-41$ blend indicates that the emission is not formed in the photosphere of either component. The variations of the line intensities (Fig. 8) indicate that the two emission peaks have contributions arising from distinct physical regions of the winds.

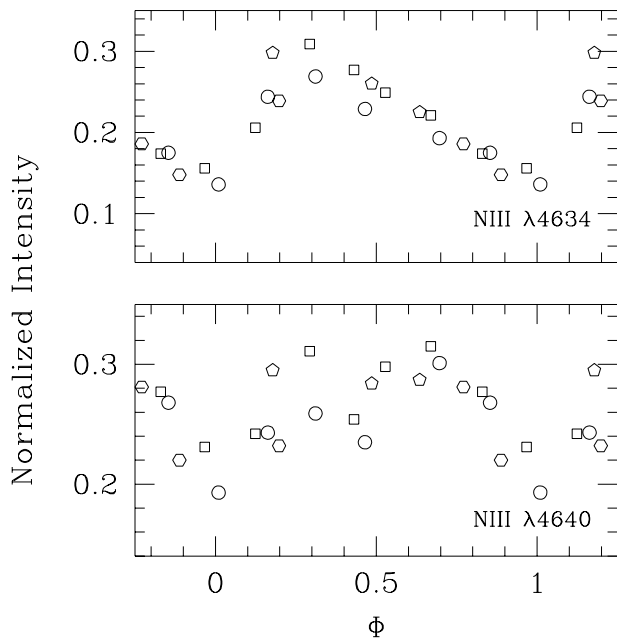


FIG. 8.—Variations of the normalized intensity of the N III $\lambda 4634$ (top) and $\lambda\lambda 4640-4641$ (bottom) emission peaks. The intensities were “corrected” for the varying continuum level using the B light curve of Leung & Schneider (1978).

We have also measured the RVs of the Si IV emission lines at $\lambda\lambda 4089, 4116$ and $\lambda\lambda 6668, 6701$. An S-wave analysis of the Si IV lines yields results similar to those for the He II $\lambda 4686$ line (Table 4), indicating that these lines probably arise in the same physical region.

In contrast to the characteristic Of emission features discussed so far, for which the RV analysis indicates that these emissions are mainly formed in an interaction region between the two stars, the C III $\lambda 5696$ line exhibits a radically different behavior. In fact, the radial velocity of this line is nearly in phase with the orbital motion of the primary star, although the amplitude of variation is slightly lower (Table 4). We also notice a considerably more negative systemic velocity for this line than for the other emis-

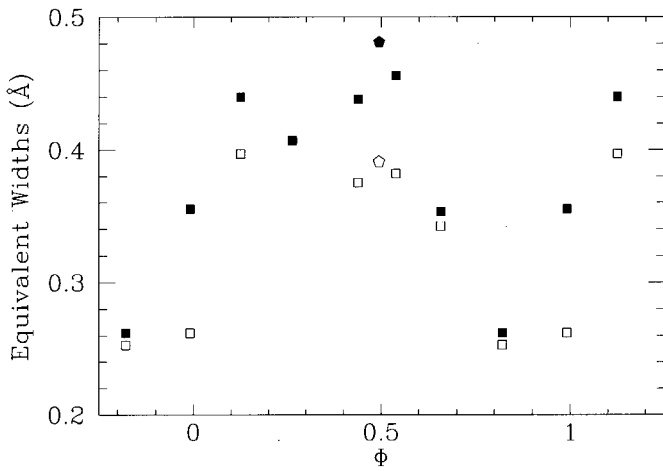


FIG. 9.—Variations of the equivalent width of the C III $\lambda 5696$ line as a function of orbital phase during our 1995 observations. Symbols have the same meaning as in Fig. 4. Open symbols represent the measurements “corrected” for the varying continuum level using the V light curve of Leung & Schneider (1978).

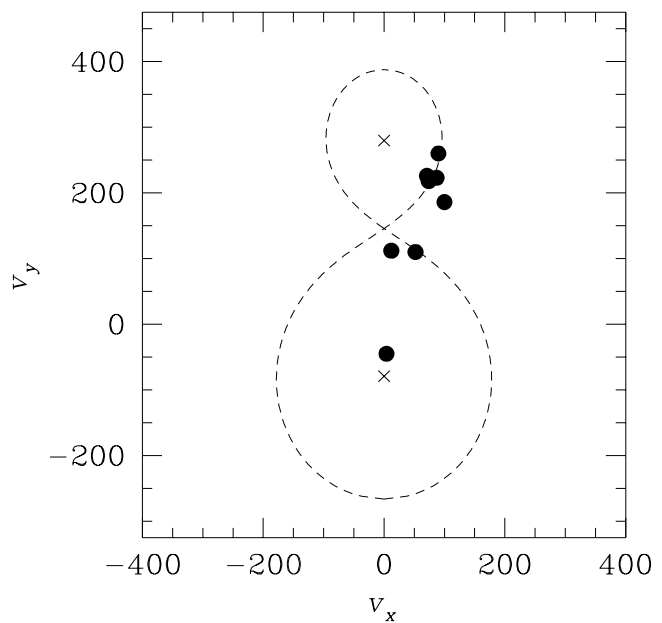


FIG. 10.—Location of the emitting volumes in the velocity space projected on the (v_x, v_y) plane (see Table 4). The dashed contour gives the shape of the “classical” Roche lobe in the velocity space. Crosses show the velocities of the centers of mass of each component. The filled circles near the inner Lagrangian point show the H β and He I $\lambda 5876$ lines.

sion lines discussed above. The equivalent width of the line integrated between $\lambda 5688.5$ and $\lambda 5700$ and corrected for the variations of the continuum level is shown in Figure 9. There is a broad minimum in the light curve around $\phi = 0.9$, whereas we see no trace of a secondary minimum.

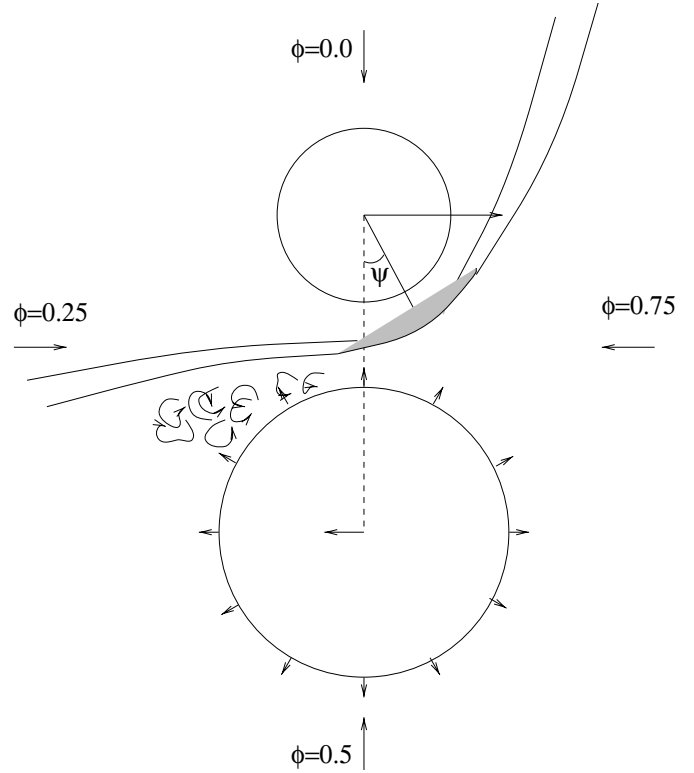


FIG. 11.—Schematic view of the wind interaction in BD +40°4220. The shaded region indicates the He II $\lambda 4686$ emitting zone. The curved arrows illustrate the velocity field of the primary’s wind that is affected by the proximity of the shock front.

The C III $\lambda 5696$ line profile is rather symmetric all over the orbital cycle, but displays some variations of its FWHM. At $\phi = 0.263$, we measure a FWHM of 350 km s $^{-1}$, while at the other orbital phases we find a width of the order of 200 km s $^{-1}$. This phenomenon is reminiscent of the widening of the primary's H β and He I $\lambda 5876$ absorptions between phases 0.2 and 0.3.

Cardona-Núñez (1978) has studied the emission process of the C III $\lambda 5696$ ($3p\ 1P^0$ – $3d\ 1D$) transition in Of stars, showing that this line can get into emission in the photospheres of these stars. An extended atmosphere enhances the emission, but is not a necessary condition for its existence.

Our S-wave analysis indicates that the C III $\lambda 5696$ emission in the spectrum of BD +40°4220 has nearly the same velocity coordinates as the center of mass of the primary star (see Table 4 and Fig. 10). The similarity between the width changes of the C III emission and those of the absorption lines provides further evidence that this emission line indeed forms in the primary's photosphere. The changing line width is most likely related to an increase of the turbulence in the deeper layers of the primary's wind, caused by the proximity of the shock region (see Fig. 11 and the discussion on the H β line).

5. DISCUSSION OF THE RV ANALYSES

The location of the centers of emission of the various lines we have analyzed in the velocity space (v_x, v_y, v_z) is summarized in Table 4. Figure 10 shows a schematic view of these results projected onto the (v_x, v_y) plane. One has to bear in mind that the fact that two emission volumes share the same coordinates in the velocity space does not necessarily mean that they have identical locations in the geometrical space. Nevertheless, Figure 10 shows that, apart from the C III $\lambda 5696$ line, most of the emission lines display a behavior quite similar to that of the He II $\lambda 4686$ line, i.e., the matter producing the emission is moving from the primary toward the secondary ($v_x > 0$) and is located on the same side of the center of gravity as the secondary ($v_y > 0$). Therefore, the majority of the emission lines are probably formed at least partially in the interaction region between the two stars.

Figure 11 provides a schematic illustration of a colliding winds interaction in BD +40°4220. Since we find that the interaction region is located close to the secondary's surface, the primary's wind most probably dominates that of the secondary star, and the shock is wrapped around the secondary (e.g., Stevens et al. 1992). The collision of the two winds leads to an important increase of the density behind the shock, allowing recombination lines to form. Given the short orbital period, the Coriolis forces will bend the shock around the secondary star, and the stagnation point is located off the axis of the binary system by some $\psi = 20^\circ$ (§ 4.1). The latter picture is in good agreement with the model of Vreux (1985), who found an off-axis angle of 22.5° for the location of the H α emitting volume. Given the proximity of the two stars and the importance of the Coriolis forces, we further expect the primary's wind to become turbulent in the vicinity of the trailing arm of the shock front (Fig. 11).

As a consequence of the wind collision, a considerable amount of energy is released, and the plasma in the vicinity of the shock is heated to high temperatures, leading to X-ray emission that will affect the ionization equilibrium near the stagnation point. X-rays from the interaction

region could also heat up the surface of either star and lead to an asymmetry in the formation region of those lines that are sensitive to the temperature. Chlebowski & Garmany (1991) have shown that the X-ray excess produced by colliding winds depends on the separation of the components; the closer the components, the weaker the excess, such that contact binaries show no significant excess at all. In this context, BD +40°4220 is quite different from putative contact binaries such as 29 CMa, AO Cas, and RY Sct. In fact, BD +40°4220 is a rather bright X-ray source ($\log L_X/L_{bol} = -5.85 \pm 0.48$; Chlebowski 1989), whose X-ray luminosity exceeds that expected from the canonical ratio ($\log L_X^{\text{single}}/L_{bol} \sim -6.55$; Chlebowski & Garmany 1991) by a factor of 5. However, the existing *ROSAT* observations do not reveal any clear phase-locked variability of the X-ray flux (Corcoran 1996; M. F. Corcoran 1998, private communication). The lack of significant variability could indicate that the bulk of the X-ray emission is related to the nonthermal radio emission of the system (e.g., Miralles et al. 1994) rather than to the colliding winds phenomenon in the short-period binary system. Like the nonthermal radio emission (Contreras et al. 1997), part of the X-ray emission could thus be produced in the interaction zone between the winds of the visual components.

In summary, we can say that

1. The line profile variability of the strongest emission lines is linked to the orbital motion of the close binary and is stable over timescales of about 10 yr, i.e., between the observations of Vreux (1985) and ours (see, however, the case of the H β line).
2. The S-wave analysis of the emission lines indicates that a sizeable fraction of the emitting matter is moving from the primary toward the secondary.
3. The interaction region is located between the two components of the close binary and close to the surface of the secondary star, slightly preceding the secondary on its orbital motion.

6. MODELING THE LINE PROFILE VARIABILITY

In this section, we discuss a numerical code for computing synthetic line profiles of a colliding winds binary. We use the constraints derived in § 5 to build a model of the wind interaction in BD +40°4220, and we compare the synthetic profiles to the observed variations of the He II $\lambda 4686$ emission.

The simulation of line profile variability in a colliding wind binary is a very complex problem. Generally speaking, the two winds may differ in their velocity laws, their ionization structure, their density, and their chemical composition. Moreover, each of the two stars has its own radiation field, which will influence the ionization balance of both winds as well as the dynamics of the interaction (Gayley et al. 1997). Therefore, a complete handling of the problem requires a simultaneous resolution of the hydrodynamical problem and the radiation transfer equations under the constraint of statistical equilibrium. Such a treatment is beyond the scope of the present paper. We limit ourselves to the problem of radiation transfer, adopting an *a priori* formulation of the dynamical structure of the winds. Most of the model atmospheres of hot stars assume spherical symmetry. However, in a binary system, this assumption obviously breaks down because of the presence of the second

star, and a complete modeling requires in principle a three-dimensional treatment. Previous attempts to model line profile variations in a colliding winds binary have been presented by Stevens (1993) and Lührs (1997). Stevens (1993) used Monte Carlo techniques to simulate the variability of resonance lines in an axisymmetric geometry, but neglecting the contribution of the interaction region. On the other hand, Lührs (1997) computed synthetic profiles resulting from the sole surplus emission produced by the gas compressed in the interaction cone.

In the following discussion, we make use of the simplified axisymmetric model developed by Rauw (1997). We suppose that the interaction region is symmetric around the binary axis and that the velocity fields outside the shock region are spherically symmetric and can be described by simple β laws:

$$v_i(r) = v_{0,i} + (v_{\infty,i} - v_{0,i}) \left(1 - \frac{R_{*,i}}{r}\right)^{\beta_i}, \quad i = 1, 2,$$

where $R_{*,i}$ are the radii of the two stars. The density in the unperturbed parts of the winds follows from the mass continuity equation.

In our model, we assume that the interaction region is limited by two cones with opening angles θ_1 and θ_2 . We therefore neglect the deflection of the shock due to the effects of the Coriolis forces. Figure 12 presents a schematic view of our model of the wind collision.

The collision of two hypersonic winds heats the plasma up to temperatures of the order of 10^8 K (~ 4 keV), near the stagnation point. The conditions of temperature and density in the interaction zone depend on the efficiency of radiative cooling in the shocked gas (Stevens et al. 1992; Lührs 1997). If radiative cooling is negligible, the flow behind the shock is nearly adiabatic, and the interaction region is quite large. On the other hand, if radiative cooling is very efficient, the shocked plasma cools down rapidly, the interaction region is very thin, and the total compression of the gas is given by the Rankine-Hugoniot relations $\rho_{\text{shock}} = \text{Ma}^2 \rho_{\text{wind}}$. In this relation, Ma is the Mach number, $\text{Ma} = v_{\perp}/c_s$, ahead of the shock, where c_s is the speed of sound and v_{\perp} is the wind velocity perpendicular to the shock (Luo,

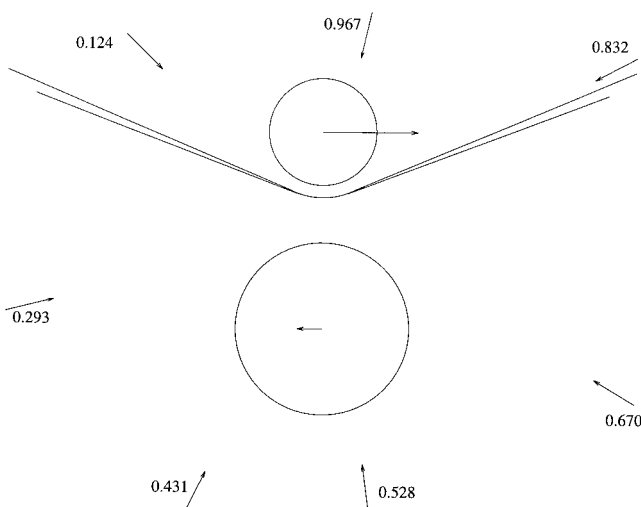


FIG. 12.—Schematic view of our model of the wind collision in BD +40°4220. The lines of sight of the 1995 July observations are projected onto the plane of the orbit.

McCray, & Mac Low 1990). The dimensions of the interaction zone follow from the density under the constraint of mass conservation (Rauw 1997).

In our model of BD +40°4220, we find a cooling parameter $\chi = (t_{\text{cool}}/t_{\text{esc}}) \ll 1$, indicating that radiative cooling is probably very efficient (Stevens et al. 1992). The gas cools down very rapidly after crossing the shock front and therefore contributes significantly to the formation of optical recombination lines.

The simulation of the observed line profiles requires a knowledge of the populations of the atomic levels involved in the corresponding transition (e.g., Klein & Castor 1978). The occupation numbers of the atomic levels are computed under non-LTE conditions in the reference plane defined by the axis of the binary and the line of sight (see Rauw 1997). To this end, we construct a two-dimensional grid in this reference plane. The resolution of the equations of statistical equilibrium through lambda iterations requires a knowledge of the local conditions of temperature and density, as well as of the mean intensities J_v , the dilution coefficients of the continuum radiation of each star, and the escape probabilities $\beta = (1/4\pi) \int_{4\pi} [(1 - e^{-\tau})/\tau] d\Omega$. In the framework of the Sobolev approximation, the optical depth measured in an arbitrary direction \mathbf{n} is given by

$$\tau = \frac{kc}{v_0} \frac{1}{|Q|}, \quad (3)$$

where

$$k = \frac{\pi e^2}{mc} (gf)_{l,u} \left(\frac{N_l}{g_l} - \frac{N_u}{g_u} \right) \quad (4)$$

and

$$Q = \mathbf{n} \cdot (\mathbf{n} \cdot \nabla) \mathbf{v} = \mathbf{n}^T \mathbf{e} \mathbf{n}. \quad (5)$$

In these relations, N and g are the occupation numbers and statistical weights of the lower (l) and upper (u) atomic levels of the transition of frequency v_0 , while f stands for the oscillator strength of the transition and \mathbf{e} is the rate-of-strain tensor (Rybicki & Hummer 1978):

$$e_{ij} = \frac{1}{2} \left(\frac{\partial v_i}{\partial x_j} + \frac{\partial v_j}{\partial x_i} \right).$$

Once the occupation numbers are known, the reference plane is rotated around the axis of the binary to build a three-dimensional grid. For each node of this grid, we compute the optical depth measured in the direction \mathbf{n}_{obs} toward the observer, and the line-of-sight velocity, $\mathbf{n}_{\text{obs}} \cdot \mathbf{v}$. The latter velocity yields the observed frequency

$$v = v_0 - \frac{v_0}{c} (\mathbf{n}_{\text{obs}} \cdot \mathbf{v})$$

of the radiation emitted at the corresponding node of the grid. Finally, to compute the line profile, we add the fluxes emitted at all the nodes corresponding to a given frequency, taking into account the visibility of the individual nodes.

Our model includes several simplifying assumptions. For instance, it does not take into account photospheric absorption lines or multiple velocity surfaces. Moreover, the adopted velocity field is quite idealistic. In real colliding winds binaries, hydrodynamical instabilities are likely to exist, leading to complex, turbulent flows (Stevens et al. 1992; Walder 1995). On the other hand, the model also

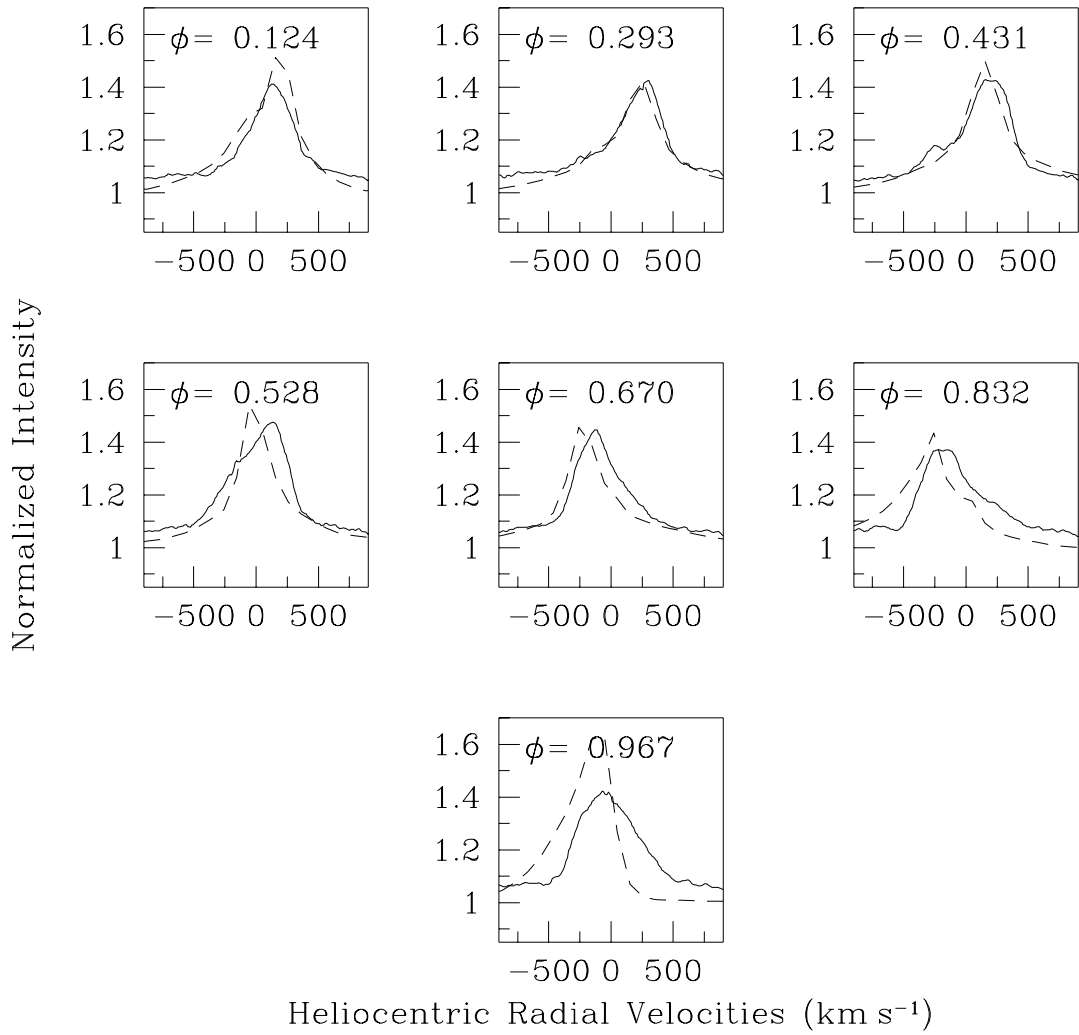


FIG. 13.—Comparison of the He II $\lambda 4686$ emission profiles observed in the spectrum of BD +40°4220 during the 1995 July run (solid lines) and the synthetic profiles computed with our model (dashed lines).

neglects the velocity dispersion of the gas resulting from the combined effects of the flight time and the orbital motion of the stars. This latter limitation mainly concerns those spectral lines that form in the outer regions of the winds (see Rauw 1997).

Given our simplifying assumptions, the important number of free parameters, and the nonlinear dependence of the phenomena on these parameters, it seems illusory to attempt an exact simulation of the observed variations at all orbital phases. This is especially true since the properties of

the winds in BD +40°4220 are poorly known. In fact, the important reddening toward the system prevents a reliable determination of the terminal velocity from observations of P Cygni profiles in the UV. Leitherer et al. (1982) propose a velocity law $v(r) = v_\infty \{0.01 + 0.99[1 - (R/r)]^\beta\}$, with $v_\infty = 1800 \text{ km s}^{-1}$ and $\beta = 1.02$, but their terminal velocity is simply an average value of a sample of O7 If stars. Values of the mass-loss rate ranging from $\dot{M} = 1.9 \times 10^{-5}$ to $2.6 \times 10^{-5} M_\odot \text{ yr}^{-1}$ have been determined by various techniques based on the H α flux, the infrared excess, or the radio

TABLE 5
PARAMETERS OF OUR COLLIDING WINDS MODEL OF BD +40°4220

Source	R_* (R_\odot)	T_{eff} (K)	X_H ^a	\dot{M} ($M_\odot \text{ yr}^{-1}$)	v_∞ (km s^{-1})	v_0 (km s^{-1})	β
Primary	27.0	36000	0.7	5.0×10^{-6}	2200	50	0.8
Secondary.....	15.5	40000	0.4	5.5×10^{-6}	600	100	0.8

NOTE.—We adopt an inclination of 50°. The interaction region is located at a distance of 39 R_\odot away from the center of the primary star and is limited by two cones of half opening angle 69° and 67°. One should be aware that the parameters listed do not agree with the photometric solution of Leung & Schneider (1978).

^a X_H is the mass fraction of hydrogen in the wind.

emission (Leitherer et al. 1982; Persí et al. 1990). Contreras et al. (1996) propose an even higher mass-loss rate of $5.47 \times 10^{-5} M_{\odot} \text{ yr}^{-1}$, derived from their radio observations. At this stage, it is worth recalling that only the thermal radio emission can be related to \dot{M} , and since BD +40°4220 is a nonthermal radio emitter, the values derived from the radio flux may overestimate the actual mass-loss rate.

Our discussion in § 5 reveals that an important contribution to the emission lines comes from a zone located close to the surface of the secondary star. Among the models we have tested, only those with the secondary having a denser wind meet this constraint. When two winds of unequal momentum flux collide, the contact discontinuity is a curved surface, with the concave side facing the star with the weaker wind. The location and shape of this contact surface largely depend on the ratio of momentum flux, $(\dot{M}_1 v_{\infty,1})/(\dot{M}_2 v_{\infty,2})$ (Stevens et al. 1992; Usov 1995). In § 5, we have shown that the interaction zone is formed by matter moving from the primary toward the secondary, and is most probably located close to the secondary's surface. We therefore conclude that the momentum flux of the primary star exceeds that of the secondary. The easiest way to meet these conditions is to assume that the mass-loss rates of both components in BD +40°4220 are comparable, while the velocity of the secondary's wind must be lower than that of the primary's wind.

In the present simulations, we have included the orbital motion of the gas *a posteriori* when calculating the line-of-sight velocity. We have assumed that the line emission follows the motion of the stars and that the interaction region corotates with the binary system (Rauw 1997). In the case of the He II $\lambda 4686$ line, these assumptions are plausible, since this line forms in the denser regions of the winds and of the interaction region.

Figure 13 illustrates the synthetic He II $\lambda 4686$ line profile variations for an inclination of 50° compared to the observations of BD +40°4220 obtained during the 1995 July observing run at OHP. The parameters of the model used to simulate these profiles are listed in Table 5. We find that some 55%–65% of the He II $\lambda 4686$ flux arise in the shock region. Figure 13 demonstrates that an important part of the observed variations can be reproduced. The agreement is quite good at phases $\phi = 0.124, 0.293, 0.431$, and 0.670. At phase $\phi = 0.670$, our model fits the shape of the observed profile but is shifted blueward with respect to the observed profile. At orbital phases $\phi = 0.528, 0.967$, and 0.832, the agreement is less satisfactory. Some of these discrepancies are probably linked to the assumption of axisymmetry and the neglect of the deflection produced by the Coriolis forces (see Rauw 1997).

Another possible weakness of our model at the present stage is that it assumes that the mass loss per unit solid angle is uniform over the entire “unperturbed” surface of the stars. We thus neglect the braking effects discussed by Stevens & Pollock (1994) and Gayley, Owocki, & Cranmer (1997), as well as the focusing of the winds (Stevens 1988). This could also account for some of the discrepancy between our model and the observations, especially at phase $\phi = 0.967$. Another point is that we neglect the effects of X-ray emission near the stagnation point on the ionizing equilibrium in the winds.

In summary, although it is quite idealistic, our model demonstrates that the bulk of the line profile variations of

the He II $\lambda 4686$ line in BD +40°4220 can be explained by a colliding winds model. Given the important number of free parameters and the simplifying assumptions of our model, the parameters in Table 5 certainly do not provide a unique solution. Nevertheless, our simulations indicate that the secondary's wind must be denser but less energetic than the primary's wind and that the overall mass-loss rate of the close binary is most probably lower than expected from the radio emission or the H α flux, i.e., by means of methods that assume smooth winds and do not account for the surplus emission from the shock region.

7. TOWARD A POSSIBLE EXPLANATION

7.1. The Primary Star

Our new orbital solution yields minimum masses of $m_1 \sin^3 i = 24.6$ and $m_2 \sin^3 i = 6.9 M_{\odot}$ for the primary and the secondary, respectively. Adopting the inclination $i = 68^{\circ}18'$ derived by Leung & Schneider (1978), this corresponds to absolute masses of $m_1 = 31$ and $m_2 = 9 M_{\odot}$. On the other hand, our analysis of the light curve of the He II $\lambda 4686$ emission yields a lower inclination between 50° and 60° (§ 4.1), corresponding to absolute masses of 38–55 M_{\odot} and 10.5–15.5 M_{\odot} for the primary and the secondary, respectively. The distance modulus and reddening toward BD +40°4220 have been evaluated to 10.71 and $A_V = 6.1$ –6.4 mag (Leitherer et al. 1982; Torres-Dodgen, Tapia, & Carroll 1991), assuming an O7 Ia^f p spectral classification (Walborn 1973). With an apparent V magnitude of 9.05 (Hall 1974) and a spectroscopic luminosity ratio of 1.4 ± 0.6 in the visible (§ 3.2), we derive absolute V magnitudes of -7.2 ± 0.3 and -7.0 ± 0.4 for the primary and secondary, respectively. Adopting the calibration of Humphreys & McElroy (1984) and assuming that the components of BD +40°4220 are indeed supergiants of spectral type O6.5–7 and O6, we obtain bolometric magnitudes of -10.6 ± 0.3 and -10.5 ± 0.4 and radii of 26.9–35.4 and 22.6–32.6 R_{\odot} for the primary and the secondary, respectively. Comparing these radii to the dimensions of the classical Roche lobes, $R_{RL,1} \sin i = 22.9 R_{\odot}$ and $R_{RL,2} \sin i = 12.9 R_{\odot}$ (see Table 2), we notice that an inclination of $i \leq 58^{\circ}$ is necessary to make the primary fit within its critical volume, whereas the inclination required to avoid Roche lobe overflow of the secondary ($i \leq 35^{\circ}$) yields completely unrealistic values of m_1 .

One might wonder how secure the Ia luminosity classification (Walborn 1973) is. In fact, we have shown that a sizeable fraction of the line emission in the spectrum of BD +40°4220 arises in the interaction region and is not intrinsic to the stars themselves. Since these emission lines provide the luminosity criterion used by Walborn (1971), the luminosity class for the primary could be in error, and the actual classification could be Ib instead of Ia. However, a lower luminosity class of the primary does not harmonize with the distance of the Cyg OB2 association (Rauw 1997).

7.2. The Secondary Star

If we suppose that the primary is indeed a normal O6–7 Ia star, we are forced to admit that the secondary is not a genuine O6 Ia star, since neither its mass nor its dimensions agree with such a spectral classification.

The secondary could be an intrinsically cooler star that mimics the spectrum of an O6 supergiant. Such a situation could result if BD +40°4220 were a contact binary in

thermal equilibrium (Kähler 1995) or if the secondary were heated by X-ray emission from the wind collision. However, these explanations cannot account for the discrepancy between the radius of the secondary, required to explain its luminosity, and the dimensions of its critical volume (Rauw 1997).

An alternative explanation is that the secondary could be an evolved object, as was suggested by Bohannan & Conti (1976) and Vreux (1985). Smith & Maeder (1989) propose a mass–absolute visual magnitude relation for Wolf-Rayet stars. From this relation, we find that a mass between 54 and 93 M_{\odot} is needed to account for an absolute visual magnitude between -6.6 and -7.4 . However, the relation of Smith & Maeder (1989) assumes a bolometric correction of -4.5 , whereas the average value of the bolometric correction derived from the model atmospheres of nine Ofpe/WN9 transition stars in the LMC is -2.8 (Crowther & Smith 1997). Adopting the latter value of the bolometric correction, the relation of Smith & Maeder (1989) yields a mass between 17 and 24 M_{\odot} , while the mass-luminosity relation of pure helium stars (Langer 1989) yields 20–32 M_{\odot} . Ofpe/WN9 stars have visual magnitudes that are compatible with that of the secondary star in BD +40°4220. Therefore, if we assume a sufficiently low (but still realistic) inclination, such a spectral classification allows us to account for the overluminosity of the secondary in BD +40°4220. Transition stars display spectral characteristics that are intermediate between those of Of stars and very late WN stars (Bohannan & Walborn 1989). Therefore, such a classification of the secondary star further allows us to account for several of its spectral features. For instance, from a qualitative point of view, the spectrum of the secondary star and its shocked wind is reminiscent of that of HD 152408, an O8:Iafpe transition star studied by Crowther & Bohannan (1997).

In normal W-R + O binaries, the wind of the W-R component dominates that of its O-type companion. If we consider an Ofpe/WN9 + O6–7 Ia binary, the situation might be different. In fact, transition stars have rather slow winds, with asymptotic velocities of the order of 200–500 km s $^{-1}$ (Crowther & Smith 1997), whereas O6–7 Ia stars have much faster winds (~ 2000 km s $^{-1}$; Lamers & Leitherer 1993).

In § 6, we have seen that by adopting mass-loss rates of 5×10^{-6} and $5.5 \times 10^{-6} M_{\odot}$ yr $^{-1}$ for the primary and the secondary, respectively, we can account for a significant part of the observed variability of the He II $\lambda 4686$ line. With the parameters of Table 5, the wind of the O6–7 Ia star would indeed dominate that of the secondary. The mass-loss rate of the secondary in our model calculations is about a factor of 4 lower than the mean value of $\dot{M} = 2 \times 10^{-5} M_{\odot}$ yr $^{-1}$ of the LMC transition stars studied by Crowther & Smith (1997). However, the mass-loss rate per unit solid angle $d\dot{M}/d\Omega$ of the secondary toward the primary could be reduced as a consequence of the presence of the primary and its radiation field (Stevens & Pollock 1994).

The global mass-loss rates of our model calculations are lower than the overall mass-loss rate of the binary obtained from various techniques commonly used to derive \dot{M} for single stars (Leitherer et al. 1982; Persi et al. 1990). This situation most probably results from the fact that the enhanced density in the wind collision zone produces excess line emission that is not accounted for in these classical techniques. A lower global mass-loss rate will also have important consequences for the interpretation of the radio observations of Contreras et al. (1997). As a matter of fact, the colors of the visual companion, located at 0.948 from the close binary, indicate that it is most probably a B0 V star. Adopting the global mass-loss rate from our model yields a much better agreement between the observed position of the nonthermal radio emission and the position expected from the typical mass-loss rate of a B0 V star (Rauw 1997).

We conclude that an Ofpe/WN9 star with appropriate physical parameters could explain many of the observed features of the secondary star in BD +40°4220. One of the remaining problem is the radius of the star. Indeed, the models of Crowther & Smith (1997) yield radii that are larger than the critical radius of the secondary star, but the radii of W-R stars derived from such standard model atmospheres are still a matter of debate.

It seems very likely that mass transfer has played a significant role in the evolution of BD +40°4220 (Sybesma 1986a). However, only those evolutionary models that predict a mass transfer occurring early during the main sequence can account for the extreme present-day mass ratio of the system (Sybesma 1986b; de Loore & Vanbeveren 1994; Rauw 1997). This, however, is only possible if the initial orbital period of the binary is very short, most probably shorter than about 2 days (Sybesma 1986b). Once the mass transfer completed, the orbital period increases as a consequence of the mass loss due to the stellar winds. New dedicated evolutionary models taking into account the effects of nonconservative Roche lobe overflow in a system where radiation pressure plays a crucial role are needed to explain the evolutionary status of BD +40°4220.

We wish to express our thanks to J. Manfroid for taking some of the OHP spectra. We are greatly indebted to the Fonds National de la Recherche Scientifique (Belgium) for multiple supports. This research is also supported in part by contract ARC 94/99-178 “Action de recherche concertée de la Communauté Française” (Belgium) and by contract P4/05 “Pôle d’Attraction Interuniversitaire” (SSTC-Belgium). Partial support through the PRODEX XMM-OM Project is also gratefully acknowledged. Travel to OHP for the observing runs was supported by the Ministère de l’Enseignement Supérieur et de la Recherche de la Communauté Française. The SIMBAD database has been consulted for the bibliography.

REFERENCES

- Abbott, D. C., Bieging, J. H., & Churchwell, E. 1981, ApJ, 303, 239
- Baranne, A., et al. 1996, A&AS, 119, 373
- Blake, C. C., Marlborough, J. M., Walker, G. A. H., & Fahlman, G. G. 1995, AJ, 109, 2698
- Bohannan, B., & Conti, P. S. 1976, ApJ, 204, 797
- Bohannan, B., & Walborn, N. R. 1989, PASP, 101, 520
- Cardona-Núñez, O. 1978, Ph.D. thesis, Univ. Colorado, Boulder
- Chlebowski, T. 1989, ApJ, 342, 1091
- Chlebowski, T., & Garmann, C. D. 1991, ApJ, 368, 241
- Conti, P. S. 1973, ApJ, 179, 181
- Conti, P. S., & Ebbets, D. 1977, ApJ, 213, 438
- Contreras, M. E., Rodríguez, L. F., Gómez, Y., & Velázquez, A. 1996, ApJ, 469, 329
- Contreras, M. E., et al. 1997, ApJ, 488, L153
- Corcoran, M. F. 1996, Rev. Mexicana Astron. Astrofis. Serie de Conf., 5, 54
- Crowther, P. A., & Bohannan, B. 1997, A&A, 317, 532
- Crowther, P. A., & Smith, L. J. 1997, A&A, 320, 500
- de Loore, C., & Vanbeveren, D. 1994, A&A, 292, 463

Drechsel, H., Haas, S., Lorenz, R., & Gayler, S. 1995, *A&A*, 294, 723

Eggleton, P. P. 1983, *ApJ*, 268, 368

Gayley, K. G., Owocki, S. P., & Cranmer, S. R. 1997, *ApJ*, 475, 786

Gies, D. R., Bagnuolo, W. G., Jr., & Penny, L. R. 1997, *ApJ*, 479, 408

Gillet, D., et al. 1994, *A&AS*, 108, 181

Hall, D. S. 1974, *Acta Astron.*, 24, 69

Herbig, G. H. 1967, *PASP*, 79, 502

Humphreys, R. M., & McElroy, D. B. 1984, *ApJ*, 284, 565

Hutsemékers, D. 1988, Ph.D. thesis, Univ. Liège

Kähler, H. 1995, *A&A*, 294, 497

Klein, R. I., & Castor, J. I. 1978, *ApJ*, 220, 902

Kondo, Y. 1996, *Rev. Mexicana Astron. Astrofis. Serie de Conf.*, 5, 5

Lamers, H. J. G. L. M., & Leitherer, C. 1993, *ApJ*, 412, 771

Langer, N. 1989, *A&A*, 210, 93

Leitherer, C., Hefele, H., Stahl, O., & Wolf, B. 1982, *A&A*, 108, 102

Leung, K.-C., & Schneider, D. P. 1978, *ApJ*, 224, 565

Lubow, S. H., & Shu, F. H. 1975, *ApJ*, 198, 383

Lührs, S. 1997, *PASP*, 109, 504

Luo, D., McCray, R., & Mac Low, M.-M. 1990, *ApJ*, 362, 267

Massey, P., & Conti, P. S. 1977, *ApJ*, 218, 431

Massey, P., & Thompson, A. B. 1991, *AJ*, 101, 1408

Mihalas, D., & Hummer, D. G. 1973, *ApJ*, 179, 827

Miralles, M. P., et al. 1994, *A&A*, 282, 547

Penny, L. R. 1996, *ApJ*, 463, 737

Persi, P., Tapia, M., Rodriguez, L. F., Ferrari-Toniolo, M., & Roth, M. 1990, *A&A*, 240, 93

Rauw, G. 1997, Ph.D. thesis, Univ. Liège

Richards, M. T., Jones, R. D., & Swain, M. A. 1996, *ApJ*, 459, 249

Rybicki, G. B., & Hummer, D. G. 1978, *ApJ*, 219, 654

Smith, L. F., & Maeder, A. 1989, *A&A*, 211, 71

Stevens, I. R. 1988, *MNRAS*, 235, 523

———. 1993, *ApJ*, 404, 281

Stevens, I. R., Blondin, J. M., & Pollock, A. M. T. 1992, *ApJ*, 386, 265

Stevens, I. R., & Pollock, A. M. T. 1994, *MNRAS*, 269, 226

Stickland, D. J. 1997, *Observatory*, 117, 37

Swings, P. 1948, *Ann. d'Astrophys.*, 11, 228

Sybesma, C. H. B. 1986a, in *IAU Symp. 116, Luminous Stars and Associations in Galaxies*, ed. C. de Loore, A. Willis, & P. Laskarides (Dordrecht: Kluwer), 395

———. 1986b, *A&A*, 168, 147

Torres-Dodgen, A. V., Tapia, M., & Carroll, M. 1991, *MNRAS*, 249, 1

Usov, V. V. 1995, in *IAU Symp. 163, Wolf-Rayet Stars: Binaries, Colliding Winds, Evolution*, ed. K. A. van der Hucht & P. M. Williams (Dordrecht: Kluwer), 495

Vreux, J.-M. 1985, *A&A*, 143, 209

Vreux, J.-M., Rauw, G., Bohannan, B., & Manfroid, J. 1996, in *Wolf-Rayet Stars in the Framework of Stellar Evolution*, 33d Liège Int. Astrophys. Colloq., ed. J. M. Vreux et al. (Liège: Univ. de Liège, Inst. d'Astrophysique), 337

Walborn, N. R. 1971, *ApJS*, 23, 257

———. 1973, *ApJ*, 180, L35

Walder, R. 1995, in *IAU Symp. 163, Wolf-Rayet Stars: Binaries, Colliding Winds, Evolution*, ed. K. A. van der Hucht & P. M. Williams (Dordrecht: Kluwer), 420